Compact 2×2 Automotive MIMO Antenna Systems for Sub-6 GHz 5G and V2X Communications

Ahmad Yacoub*, Mohamed Khalifa, and Daniel N. Aloi

Abstract—Various multiple-input multiple-output (MIMO) antenna systems for automotive applications are presented in this paper using two uniquely designed elements: 1) a low profile wideband Planar Inverted-F antenna (PIFA), and 2) a compact wideband monopole in the sub-6 GHz 5G systems and Vehicle-to-Everything (V2X) communications that cover the frequency range from 617 MHz to 6 GHz. The proposed MIMO systems can be used in a low-profile or shark fin style housing placed on the vehicle's roof. Each MIMO system achieves satisfactory performance across the whole band with suitable physical dimensions. The envelope correlation coefficient (ECC) and diversity gain (DG) are calculated using MATLAB in each MIMO configuration as they represent the two key factors in the MIMO performance. Simulation results are presented along with measured data on a 1-meter rolled-edge ground plane (GND) and on a vehicle's roof from properly cut metal sheet prototypes. The results are discussed in terms of VSWR, passive isolation between elements, combined radiation patterns, port-efficiencies, ECC, and DG.

1. INTRODUCTION

Introducing multiple-input multiple-output (MIMO) systems for cellular 5G and vehicle-to-everything (V2X) applications is essential to meeting the requirements of the upcoming autonomous wireless communication systems in the automotive industry. A MIMO system consists of multiple antennas at receiver and transmitter sides which allows it to increase the channel capacity, data rate, and the total throughput of the system without increasing the operating frequency band or the transmit power [1]. MIMO system also has the benefits of high reliability and low latency in a high electromagnetic scattering environment by using multiple antenna elements that transmit and/or receive independent channels assuming that these elements are highly isolated or uncorrelated [2]. The performance of a MIMO system is highly dependable on the efficient design of the MIMO antennas that should have low correlation between them and a high total antenna efficiency [3, 4].

Envelope correlation coefficient (ECC) is a key performance metric used to describe the amount of correlation being added to RF channels by the MIMO antenna system. Hence, a low value of ECC (i.e., high isolation between antenna elements) is needed to achieve the requirements of the MIMO antenna diversity. In [5], the authors describe three main ways to calculate the ECC. The first method uses only the S-parameters of the antenna elements and assumes that the antennas are lossless which in practice would not yield accurate results since most antennas are lossy. The second method also uses S-parameters of the antenna elements, but it adds port efficiencies of each antenna which gives a more practical result. However, this improvement only works when the efficiency of each antenna element is better than 60%. The third method, which is used in this paper, analyzes the radiation patterns of the

electric field of each antenna element and the spatial power distribution of the signal to calculate the ECC which gives more accurate and effective results than the first two methods [5].

There are multiple challenges for MIMO antenna design in the automotive industry. It usually suffers from lack of physical space and interference between different antennas in a single housing package. So, these limitations impact the isolation and correlation between MIMO antennas and make it challenging to design an antenna system to meet the isolation and diversity requirements. Moreover, one single package usually contains multiple applications at the same time, for instance antenna elements for the cellular 5G system, global navigation satellite systems (GNSS), satellite audio digital radio system (SDARS), and V2X communication system in one limited-size module which introduces the challenges of antenna size, interference or isolation between antenna elements, and the operating bandwidth of each antenna system since these parameters are significantly affected by the physical volume [6, 7].

In this paper, multiple 2×2 MIMO antenna configurations have been analyzed for automotive applications in the 5G and V2X frequency bands. The first configuration consists of two low-profile PIFA antennas separated by a spatial distance on the vehicle's roof. The second configuration has two PIFAs within the same printed circuit board (PCB) with different rotational positions. The third configuration has a compact wideband monopole antenna and a PIFA within the same PCB to analyze the ECC between the horizontal current introduced by the PIFA and the vertical current introduced by the monopole. Both antennas have suitable physical dimensions and operate in the sub-6 GHz 5G and V2X frequency bands (617 MHz–6 GHz) with reasonable rejection to GNSS bands which makes the proposed MIMO systems suitable to be deployed with other applications within the same package.

The work in this paper proposes three novel MIMO antenna systems with unique elements that are suitable for low profile or shark fin style housing on the vehicle's roof. Each system implements a different method for optimizing MIMO performance using spatial, rotational, or orthogonal diversity. Compared to the existing work in literature (summarized in Table 4), the MIMO systems presented in this paper cover the extended sub-6 GHz 5G bands from 617 MHz to 5 GHz in addition to the V2X band at 5.9 GHz with reasonable physical dimensions and unique features of the proposed antennas. The 5G/V2X MIMO systems also have acceptable filtering for GNSS bands which makes it compatible with different navigation systems under the same housing. Furthermore, this paper provides data comparisons between ground plane and vehicle measurements in terms of different MIMO parameters such as: ECC, diversity gain (DG), combined radiation pattern, and port efficiencies. The 2×2 MIMO systems in [12, 14, 19] consist of low-profile elements, but the frequency band covered by these systems are narrow and do not cover the extended 5G/V2X bands from 617 MHz–6 GHz. In [15], the authors present a 2×2 Nefer antenna MIMO system that operates from 700 MHz to 6 GHz, but the physical dimensions of the elements are too large, and the system does not cover B71 frequency band (617 MHz–960 MHz) that will make it more challenging in terms of antenna size and volume. In [16, 17, 21, 24], the MIMO systems present printed antenna elements on dielectric materials; however, they still do not cover the wide frequency range from (617 MHz–5 GHz), and the physical dimensions of the antennas are larger. The authors in [23] present a 2×2 MIMO system with transparent monopole antennas designed on glass material, but the elements do not cover the low and middle 5G frequency bands which will introduce the challenge of bigger volume of the antenna and degraded passive isolation.

The MIMO antenna systems in this paper are simulated using HFSS software and measured both on a 1-meter rolled-edge ground plane and on a vehicle's roof inside an anechoic chamber to provide real data for different parameters such as physical dimensions, VSWR, passive isolation, combined radiation patterns, and antenna efficiency. A MATLAB script has been developed to calculate the ECCs and DGs based on the radiation patterns of the antennas on the ground plane and on vehicle.

This paper consists of the following sections: Section 2 presents the equations used to calculate the ECC and DG. Section 3 states the design goals and requirements while Sections 4, 5, and 6 show performance analyses of three distinct MIMO architectures and illustrate the contributions of this work with respect to other research in automotive MIMO systems through a literature survey.

2. CORRELATION COEFFICIENT AND DIVERSITY GAIN CALCULATIONS

In [3, 5], the authors present an accurate and effective method to calculate ECC by using the electrical radiation pattern of each antenna element measured at certain azimuth and elevation angles, and can

be summarized in Equation (1) [3, 5, 8]:

$$\rho_{e,ij} = \left| \frac{\int_0^{2\pi} \int_0^\pi (XPR \cdot E_{\theta i} \cdot E_{\theta j}^* \cdot P_\theta + XPR \cdot E_{\phi i} \cdot E_{\phi j}^* \cdot P_\phi) \sin(\theta) \, d\theta d\phi}{\sqrt{\prod_{k=i,j} \int_0^{2\pi} \int_0^\pi (XPR \cdot E_{\theta k} \cdot E_{\theta k}^* \cdot P_\theta + XPR \cdot E_{\varphi k} \cdot E_{\varphi k}^* \cdot P_\phi) \sin(\theta) \, d\theta d\phi}} \right|^2 \quad (1)$$

where $E_{\theta i}$ and $E_{\theta j}$ are the electric field components in the elevation angle direction while $E_{\varphi i}$ and $E_{\varphi j}$ are the components in the azimuthal angle direction for antennas i and j. XPR is the cross-polarization discrimination factor that shows the difference between horizontal and vertical polarizations of the incident wave. P_θ and P_φ are the power densities for elevation and azimuth angles. Equation (1) can be simplified by assuming that XPR equals 1, and the angular power densities are uniform.

Another key parameter for measuring the performance of MIMO systems is DG which is defined as the quantified enhancement in signal-to-noise ratio (SNR) when the signals are received by the MIMO antennas and is usually calculated in dB. The DG can be calculated in Equation (2) as [9]:

$$DG = DG_0 * DF * K \quad (2)$$

where DG_0 is the diversity gain of the ideal case and is equal to $10 \, \text{dB}$ (which represents the selection combiner diversity gain of two ideal elements with 99% reliability [10]). The degradation factor (DF) shows the effect of the ECC on the diversity gain and is computed as: $\sqrt{(1 - \rho)}$. K represents the ratio of the mean effective gain (MEG) between the MIMO antenna elements ($K = MEG_i/MEG_j$). MEG is the effective gain ratio at the antenna element which represents the ratio of the received power over the incident power at that element. For a good channel characteristic, the received signal from the MIMO antenna element should satisfy the condition ($K = MEG_i/MEG_j \sim= 1$).

In this paper, the ECC is calculated using Equation (1) by measuring the electric field components in an anechoic chamber then exporting these components to a MATLAB script to implement Equation (1) for ECC and Equation (2) for DG.

3. PERFORMANCE ANALYSIS OF MULTIPLE VEHICULAR MIMO ANTENNA SYSTEMS

In this section, three different configurations for 2×2 MIMO antenna systems are presented. Each configuration is simulated using HFSS software then fabricated from properly cut metal sheets and measured on both a 1-meter rolled-edge ground plane and a vehicle's roof inside an anechoic chamber. After simulation and chamber measurements, the electric field components are extracted to compute the ECC and DG using a MATLAB script with different parametric analyses presented. Table 1 shows the general design goals and performance requirements for the automotive MIMO antenna systems in terms of VSWR, passive isolation, port efficiencies, ECC, and DG.

Table 1. Design goals and requirements.

Parameter	Value
VSWR	3.3 VSWR at 5G bands/2.5 VSWR at V2X bands
Passive Isolation	Minimum 10 dB across bands
Port Efficiencies	Minimum 40% across bands
ECC/DG	ECC lower than 0.5/DG higher than 8.6603 dB

4. TWO-ELEMENT PIFA-BASED MIMO SYSTEM WITH SPATIAL DIVERSITY

The proposed antenna design in this MIMO system is derived from a PIFA while introducing unique cuts on the horizontal plane that would increase its bandwidth without increasing the volume occupied
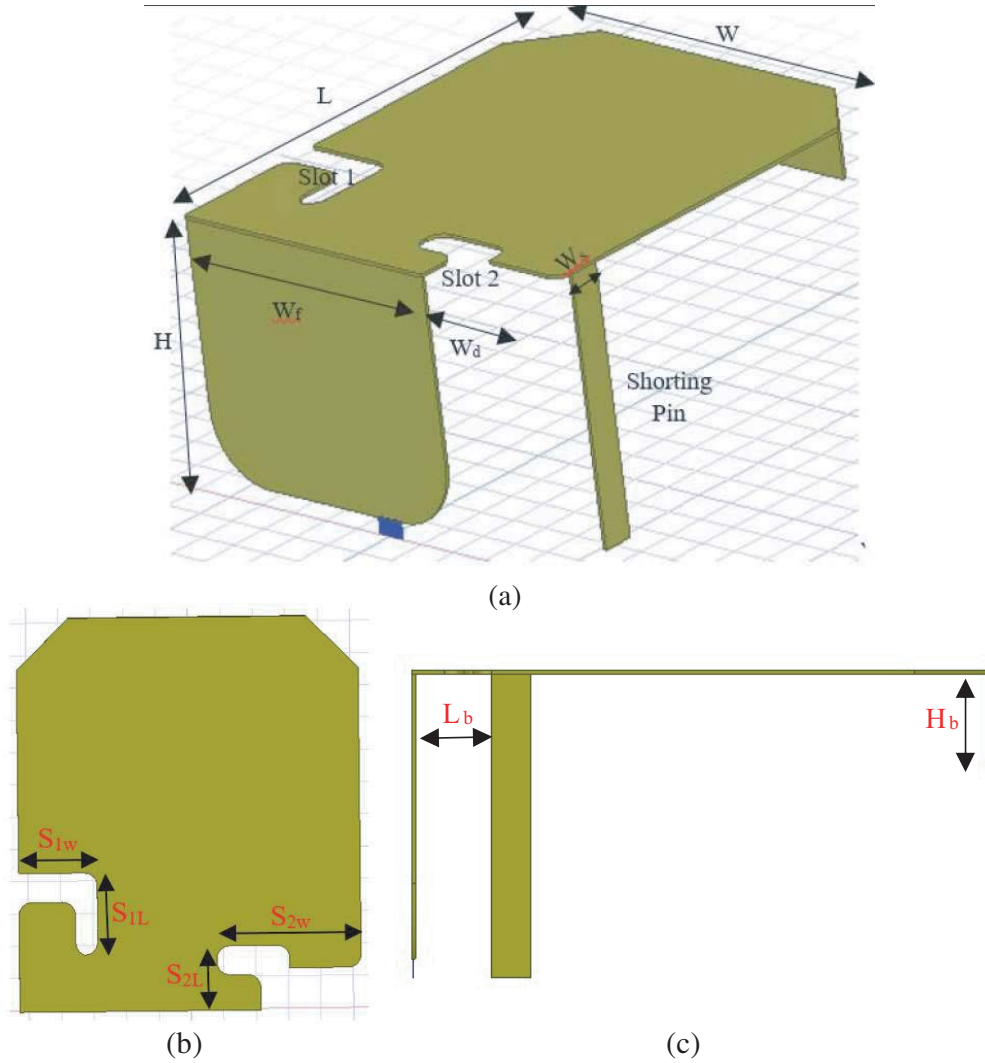
Figure 1. Antenna element model with isometric, top, and side views. (a) Isometric view. (b) Top view. (c) Side view.

by the antenna. Fig. 1 shows the PIFA element with its physical dimensions and distinct features. The wide rectangular feeding plate with width (W_f) is placed at the edge of the horizontal plane which is significant for increasing the bandwidth of the element and allows the structures of slot 1 and slot 2 to act as folded monopoles for middle and high frequency bands. A shorting pin relatively close to the feeding pin is important for the low band performance. The total volume of the structure along with the shorting pin and the extended vertical arm H_b specifies the low band center frequency $(f_c = 790 \text{ MHz})$ and bandwidth.

Structure 1 is a folded monopole structure that starts from the rectangular feeding plate and up to slot 1, and it has a radiating length of 31.25 mm which is $(\lambda/4)$ of 2.39 GHz. Structure 1 controls the frequency bands from (1.71 GHz–3.8 GHz) by optimizing the width of the rectangular plane and slot 1 width (S_{1w}). The optimized dimensions of the antenna along with structure 1 tune the element at the required bands and filter out the GNSS frequencies that reside between the low and middle 5G bands. The high frequency band from (3.8 GHz–6 GHz) is attributed to structure 2 which consists of the wide feeding plate up to slot 2. Slot 2 changes the current distribution on the horizontal plane which makes structure 2 act as a folded monopole with center frequency 5.5 GHz. The distance between the feeding plate and shorting pin (W_d) is optimized for 17.5 mm to avoid getting deep nulls in the V2X radiation patterns. Table 2 shows the values of different geometrical parameters of the antenna. An extensive

Table 2. Geometric parameters of the designed antenna.

Parameter	Value (mm)	Parameter	Value (mm)
H	28	S_{1L}	12.5
L	55	S_{2w}	22.25
W	50	S_{2L}	10
S_{1w}	12.1	W_f	29.5
W_s	6	H_b	8.5
L_b	7.5	W_d	17.5

detailed design guideline for this PIFA, its unique features compared to other elements, and its RF properties and performance are presented in full detail in our previous work in [11].

Two PIFA elements were fabricated and orientated in an opposite way (i.e., mirrored in the y-axis) to have a complementary radiation pattern for each element so that the combined pattern will be omnidirectional. The elements are then measured on 1-meter rolled-edge ground and on a vehicle's roof with 600 mm distance between them (1.25 lambda of the lowest frequency of operation "617 MHz"). Fig. 2 shows the simulation and vehicle measurement setup of the MIMO system.

The simulated VSWR for each element was captured and compared against the realized antenna measurement as depicted in Fig. 3. It is noticed that across the operating bands of 5G and V2X, the VSWR is better than 3.3 : 1 with a reasonable rejection for navigation system frequencies in the GNSS

(a)

(b)
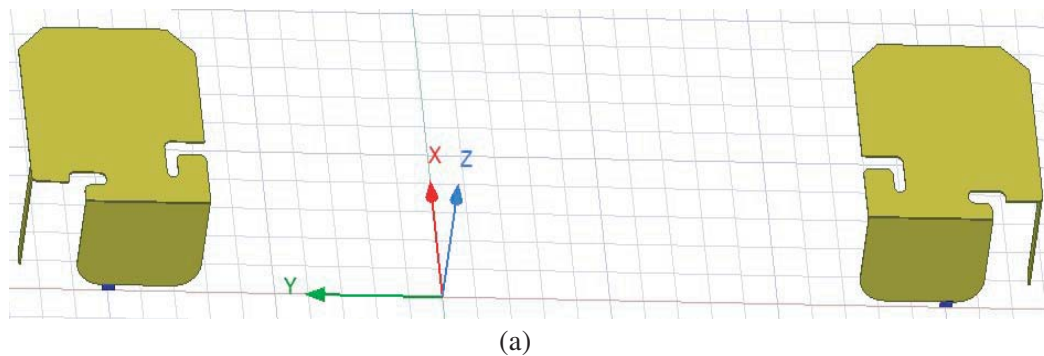
Figure 2. Simulation and vehicle measurement setup of the MIMO antennas. (a) Simulation setup. (b) Vehicle setup.
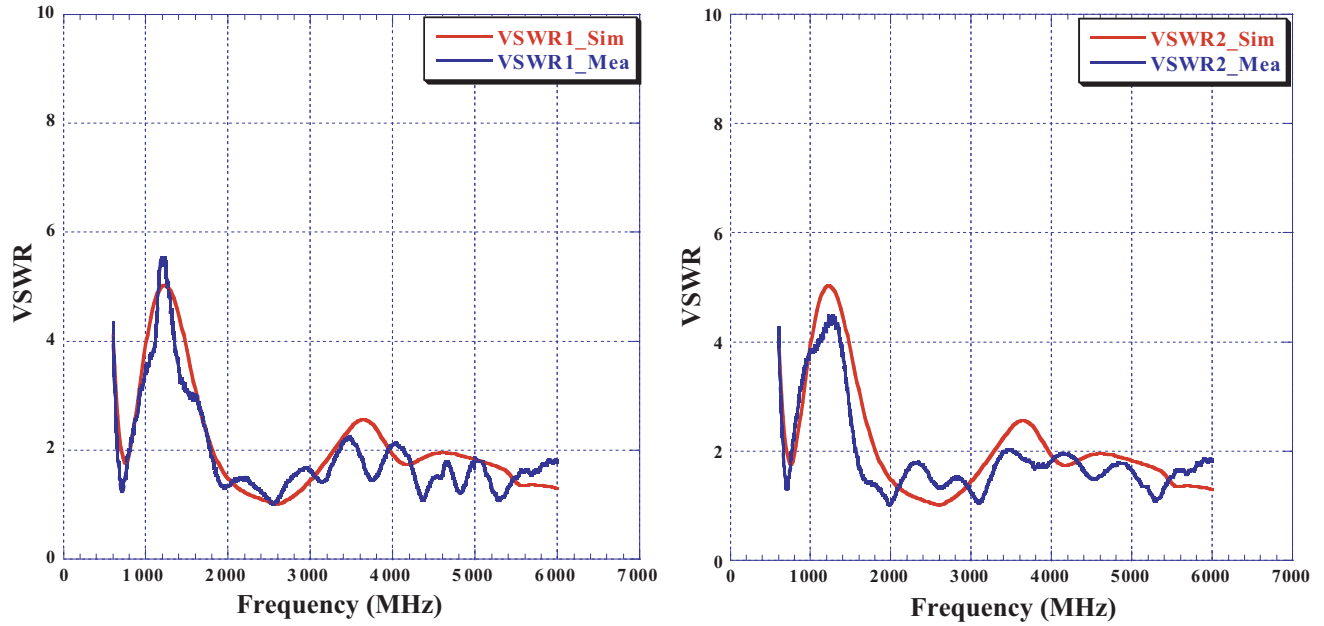
Figure 3. Simulated and measured VSWR for both elements.
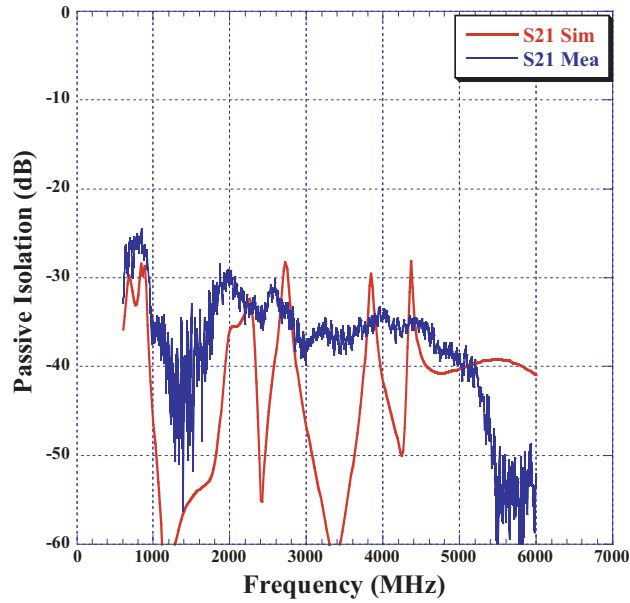
Figure 4. Simulated and measured passive isolation in dB.

bands. The passive isolation between the two PIFAs is shown in Fig. 4. The coupling between the two elements is low since they are separated by a relatively long distance (worst case isolation of 26 dB).

In Figs. 5(a), (b), (c), and (d), combined radiation patterns of horizontal cuts at theta 80 degrees are presented for frequencies 617 MHz, 1.9 GHz, 3.6 GHz, and 5 GHz while in Fig. 5(e), radiation pattern for 5.9 GHz is presented at theta 90 degrees. The patterns are measured by terminating one element by 50 ohms while measuring the other element, then the two patterns are combined to get an omnidirectional pattern around the entire vehicle. The orientation of each PIFA compared to the other is critical to get the omnidirectional behavior across the entire operating band. Moreover, the average gain observed from the combined vehicle radiation patterns is found to be −0.7 dBi, 2.1 dBi, 1.8 dBi,

and 1.1 dBi at frequencies 617 MHz, 1.9 GHz, 3.6 GHz, and 5 GHz, respectively. For V2X frequencies, the combined vehicle radiation pattern at 5.9 GHz tends to be more directive towards the back side of the car which could result from reflections caused by the roof's curvature and has a peak gain of 6.9 dBi at azimuth angle 130 degrees without having a minimum value lower than −11 dBi.

The measured radiation antenna efficiencies for the two elements on both GND and vehicle for the 5G and V2X bands are presented in Figs. 6(a), (b), (c), and (d). The radiation efficiency of each port is obtained by dividing the realized measured gain from the chamber by directivity across the whole sphere. It can be noticed that the 5G GND measurement has an average efficiency higher than 75% for both elements across all frequency bands whereas the vehicle measurement has a reduced average efficiency of 68%. For V2X frequencies, the measured antenna efficiencies on GND and on vehicle seem to have close values across the band that is higher than 70%.

The ECC and DG values for this MIMO antenna system at 5G and V2X frequencies have been calculated using a MATLAB script for Equation (1) and Equation (2) for simulation and chamber measurements. Fig. 7 shows these calculations, and it can be noticed that the worst-case value of ECC is around 0.1 at the low frequency band since lower frequency signals support longer wavelengths which require more spacing.

(a)

(b)

(c)

(d)

(e)
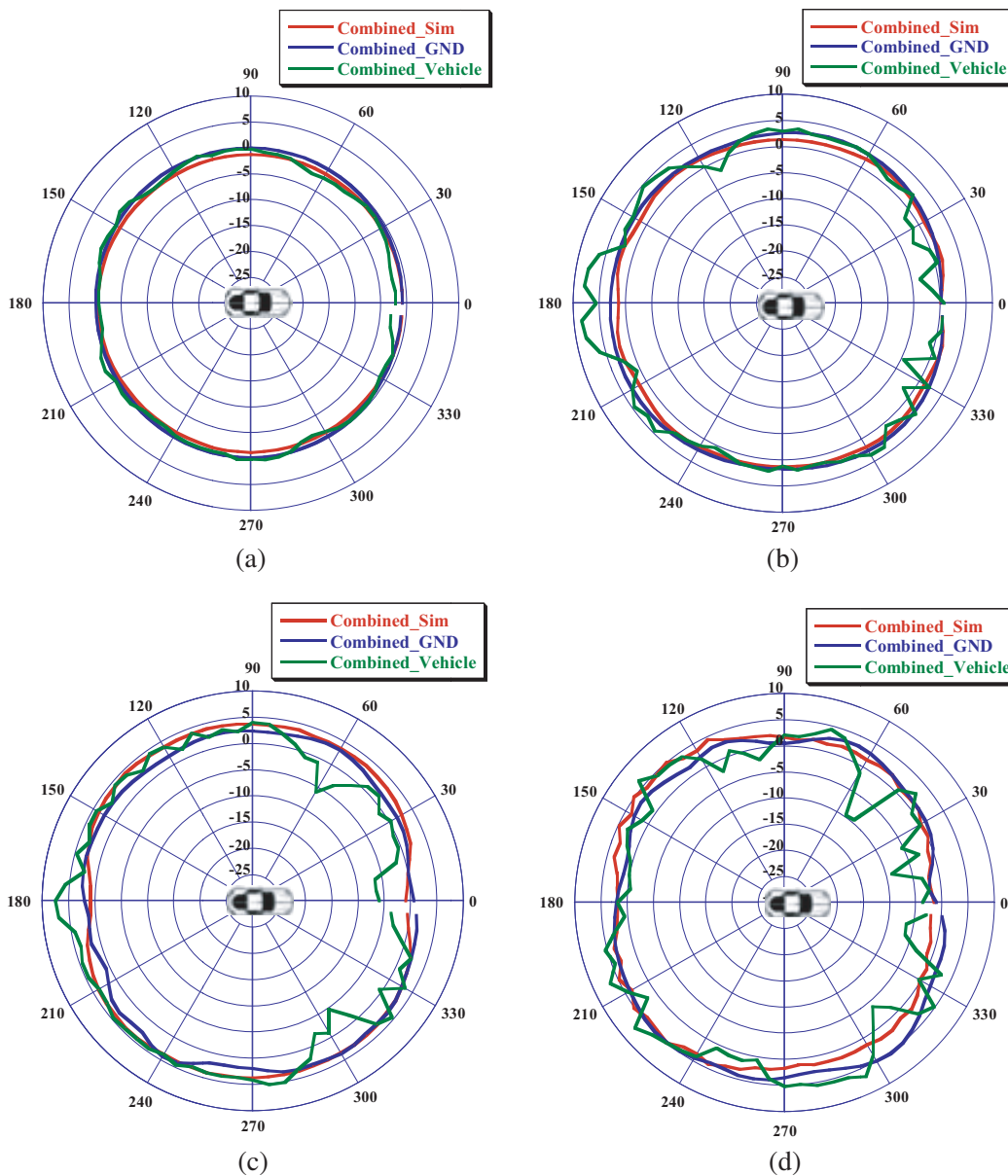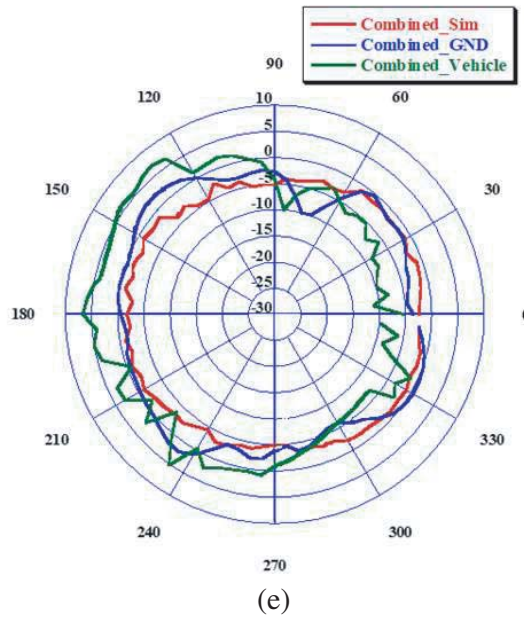
Figure 5. Combined Radiation pattern of simulation, GND measurement, and vehicle measurement in (dBi) at theta 80 deg. for frequencies: (a) 617 MHz, (b) 1900 MHz, (c) 3600 MHz, (d) 5000 MHz, and theta 90 deg. for (e) 5.9 GHz.

Next, a parametric study as function of distance between the two elements is presented using HFSS simulation. The distance is changed from 600 mm to 120 mm, 240 mm, and 480 mm. The electric field components are exported from each configuration and then processed in MATLAB to see the effect on ECC and DG. Fig. 8 shows these calculations, and it can be noticed that increasing the distance in this configuration improves the ECC and DG which gives better MIMO performance; however, the size of

(a)

(b)
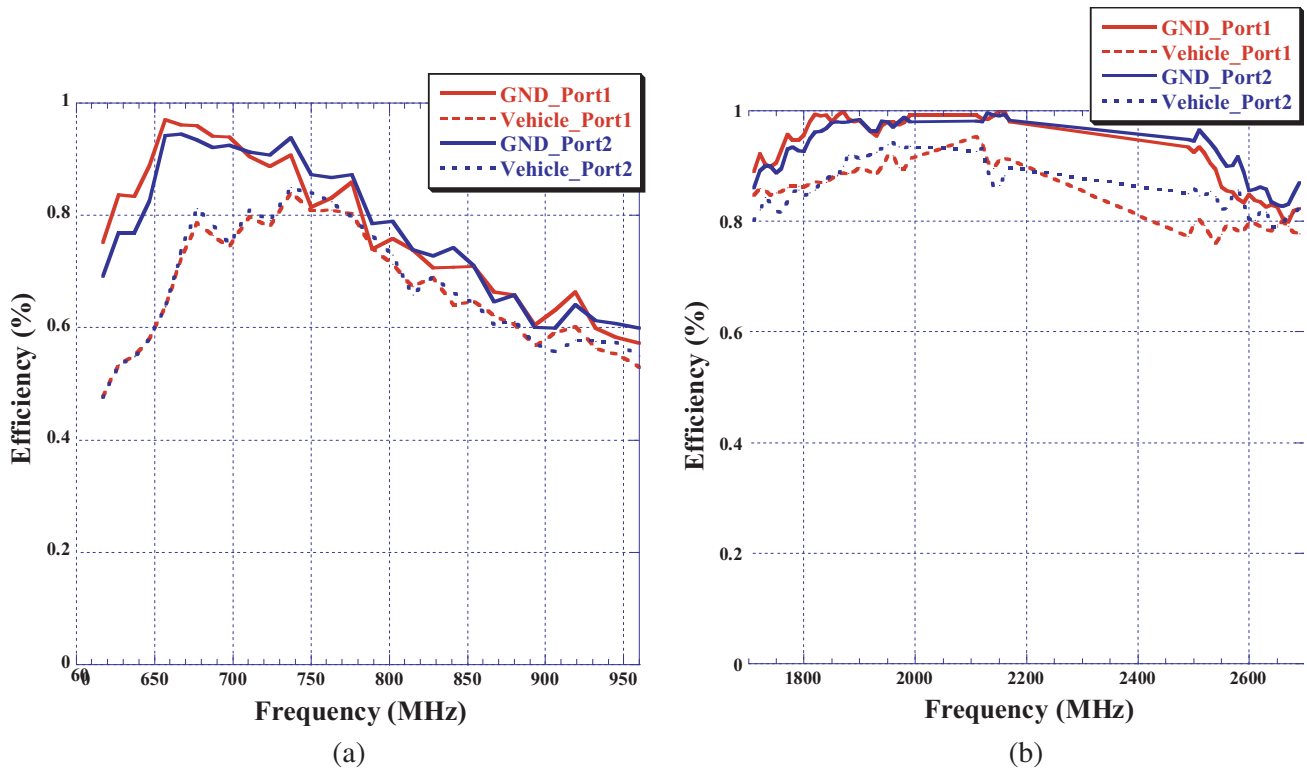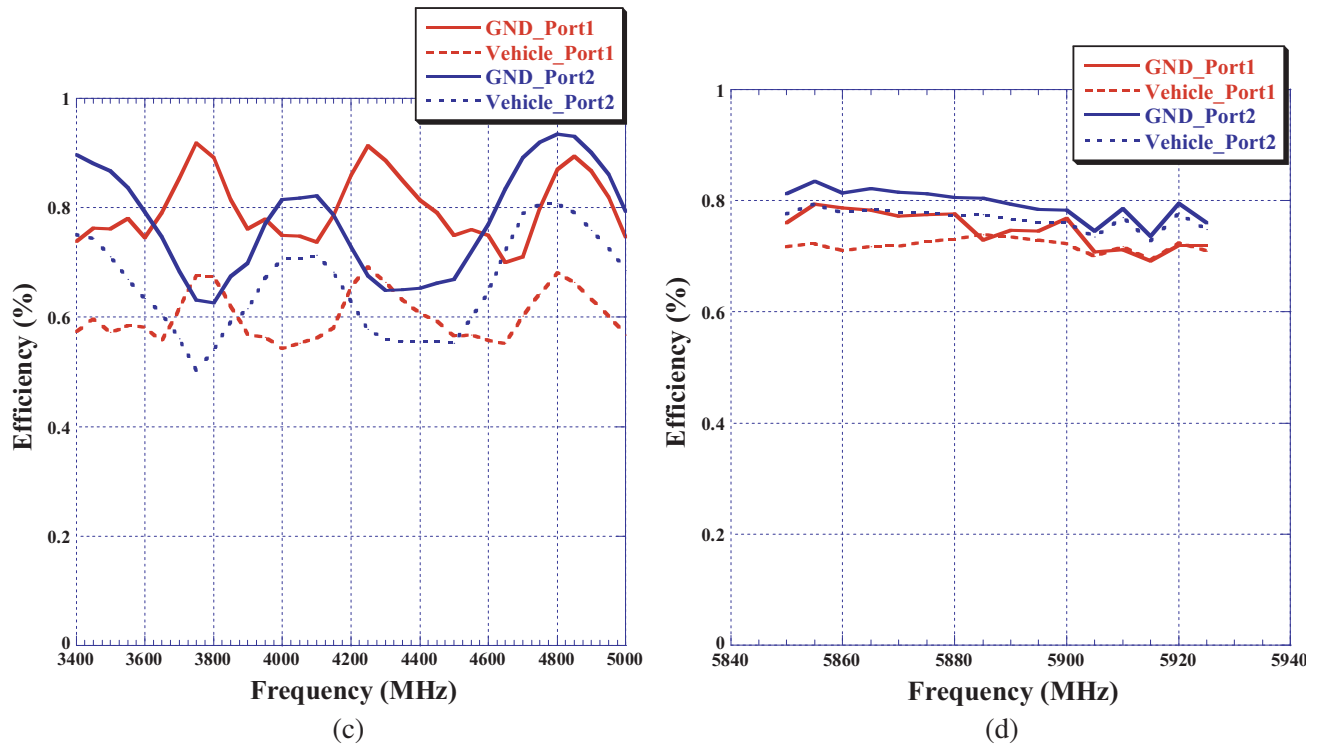
Figure 6. Antenna radiation efficiency for the two PIFAs measured on ground plane and on vehicle for 5G and V2X frequencies: (a) 617 MHz–960 MHz, (b) 1710 MHz–2690 MHz, (c) 3400 MHz–5000 MHz, (d) 5850 MHz–5925 MHz.
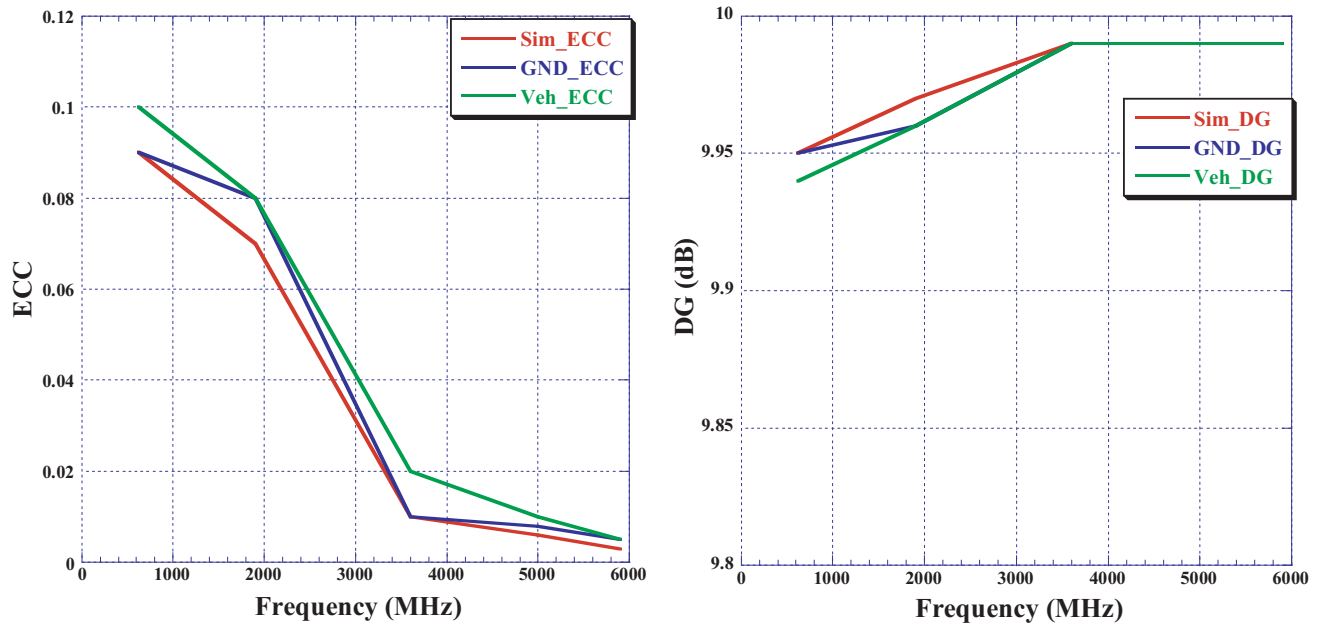
Figure 7. ECC and DG values for spaced MIMO system.

the vehicle's roof might be a limitation, and the antennas should be placed a bit further away from the edges to avoid scattering effects and exhibit reliable grounding.
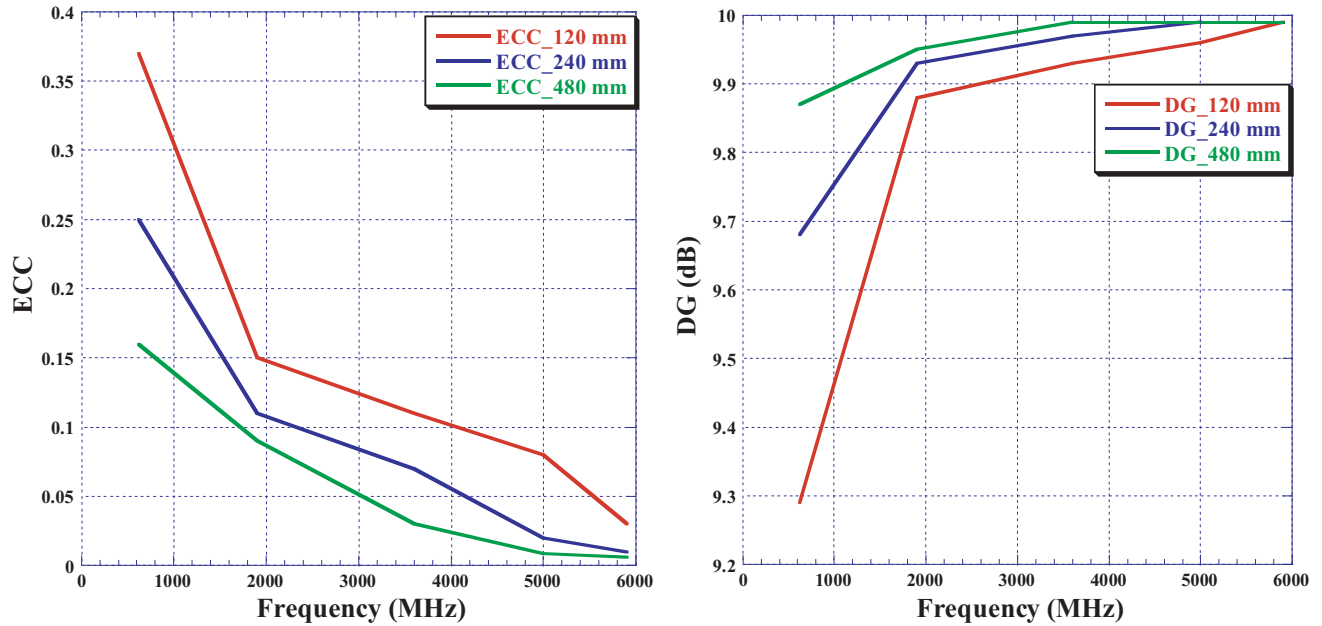
Figure 8. ECC and DG values for different distances.

5. TWO-ELEMENT PIFA-BASED MIMO SYSTEM WITH ROTATIONAL DIVERSITY

In this section, the two PIFA elements were placed on the same PCB with a physical separation of 120 mm between them (0.25 lambda of the smallest operating frequency "617 MHz"). The elements are oriented in an opposite way to have a complimentary radiation pattern that results in a combined omnidirectional pattern. The simulation and vehicle measurement setup for this configuration is shown in Fig. 9. The elements are placed in the back center of the roof as in low-profile housing module.

(a)   (b)
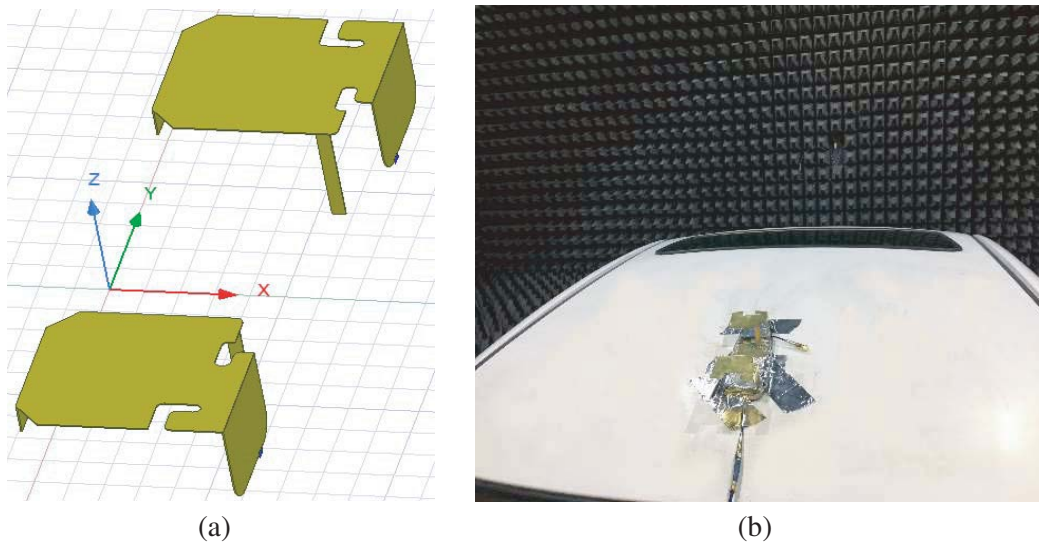
Figure 9. Simulation and vehicle measurement setup of the rotational PIFAs. (a) Simulation setup. (b) Vehicle setup.
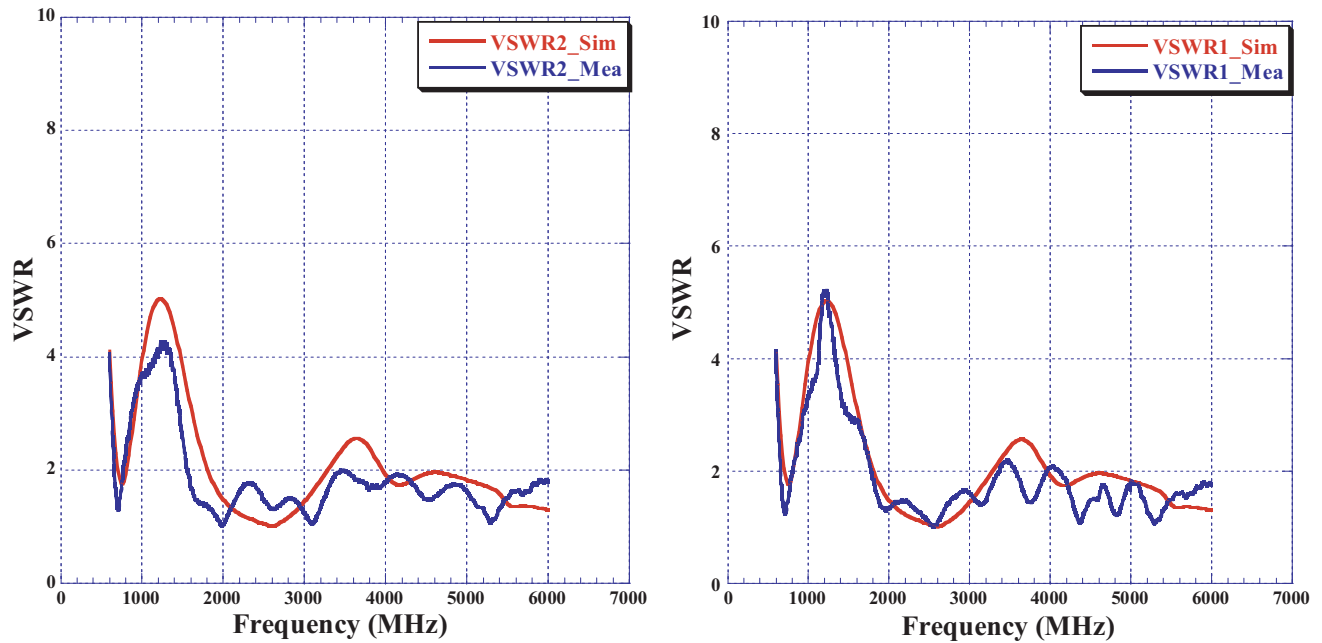
Figure 10. Simulated and measured VSWR of both elements.
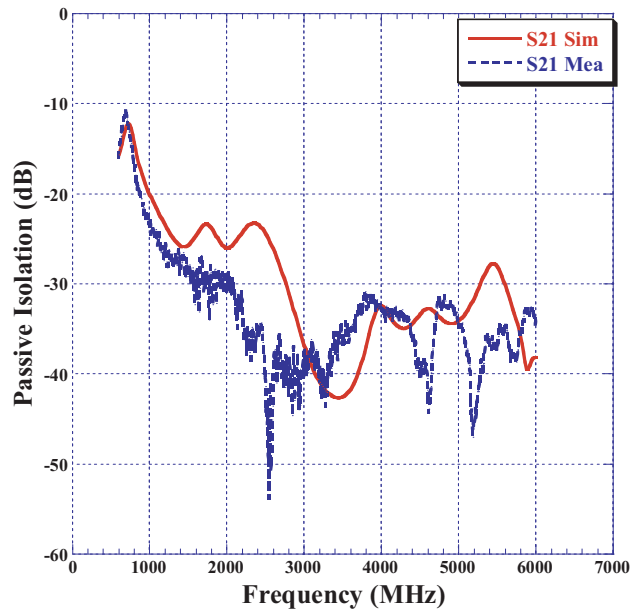
Figure 11. Simulated and measured passive isolation in dB.

The simulated VSWR for each element in this configuration is shown in Fig. 10. The VSWR is better than 3.3 : 1 across 5G and V2X bands while also having acceptable filtering for GNSS bands. The passive isolation between the two PIFAs is shown in Fig. 11. The worst coupling between the two elements has an isolation around 11 dB at the low frequency bands since they have the longest wavelength in the operating frequency range.

In Figs. 12(a), (b), (c), and (d), combined radiation patterns of horizontal cuts at theta 80 degrees are presented for frequencies 617 MHz, 1.9 GHz, 3.6 GHz, and 5 GHz while in Fig. 12(e), radiation pattern for 5.9 GHz is presented at theta 90 degrees. In reference to Fig. 9, the orientation of each element is

in the opposite side to get an omnidirectional pattern across the operating frequency range. Moreover, the average gain observed from the combined vehicle radiation patterns is found to be -1.3 dBi, 0.6 dBi, 1.4 dBi, and 1.3 dBi at frequencies 617 MHz, 1.9 GHz, 3.6 GHz, and 5 GHz, respectively. For V2X frequencies, the roof curvature of the vehicle influences the radiation pattern by making it more directive towards the backside of the car. At 5.9 GHz, the radiation pattern has a peak gain of 4.9 dBi at azimuth angle 240 degrees without having a minimum value lower than -12 dBi.

The measured radiation antenna efficiencies for the two elements are shown in Figs. 13(a), (b), (c), and (d). It can be noticed that the 5G GND measurement has an average efficiency higher than 67% for both elements while the vehicle measurement has a reduced average efficiency of 60% and higher. For V2X frequencies, the measured antenna efficiencies on the GND and on the vehicle look similar across the band with values higher than 63%.

The ECC and DG were calculated from the electric field components using Equations (1) and (2) with a MATLAB script. Fig. 14 shows these calculations with a worst-case value around 0.38 in the low frequency bands.

Simulation via HFSS was used to study the effect of element rotation on the ECC and DG. This was achieved by rotating the front PIFA in the clockwise direction in by 90, 180, and 270 degrees on the

(a)

(b)

(c)

(d)

(e)
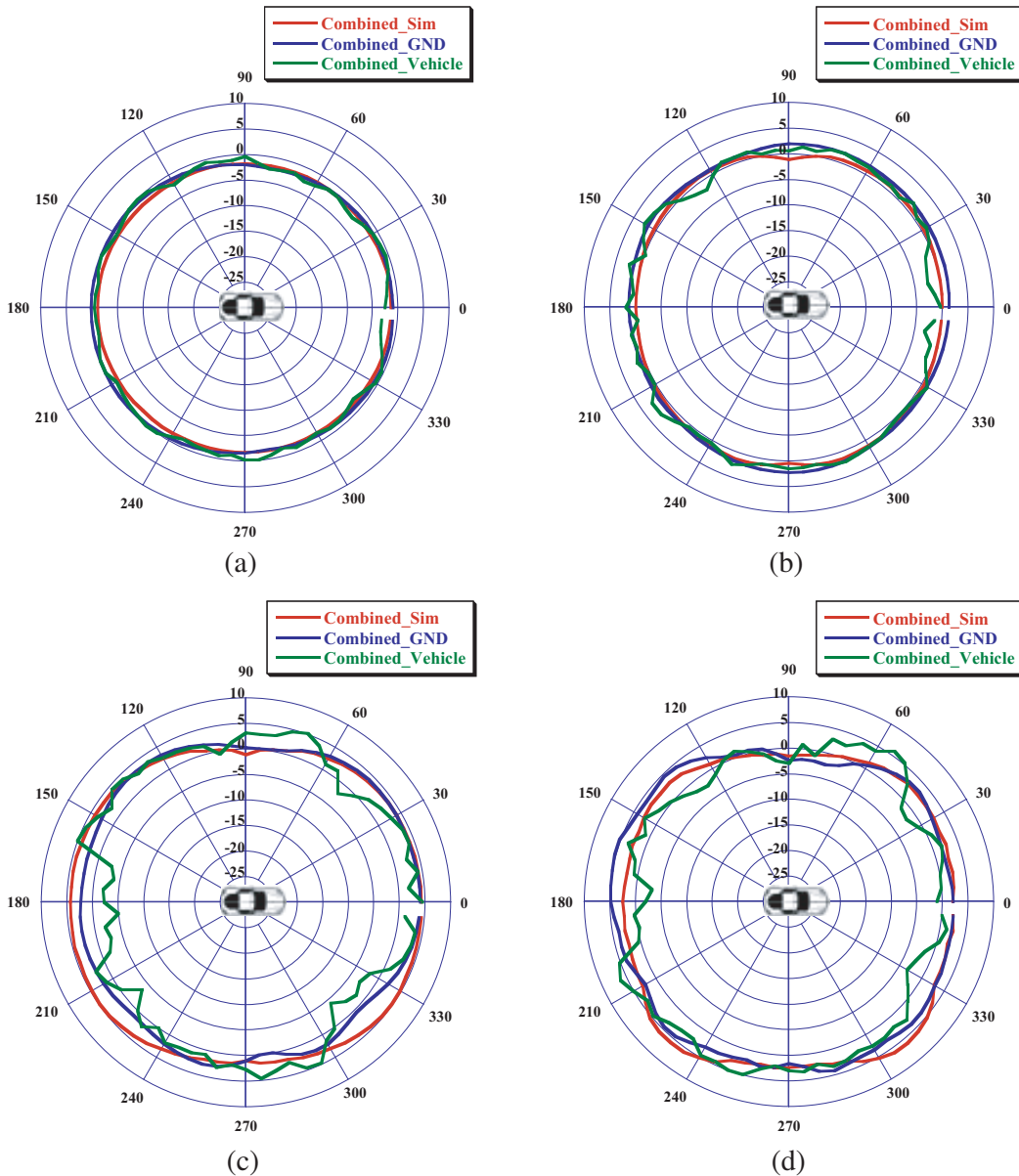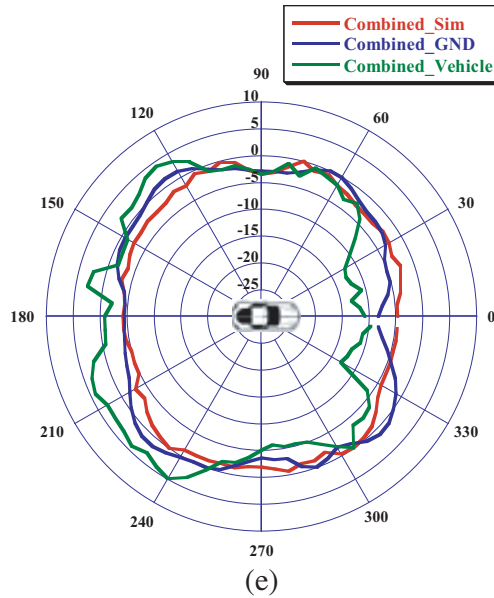
Figure 12. Combined Radiation pattern of simulation, GND, and vehicle measurement in (dBi) at theta 80 deg. for frequencies: (a) 617 MHz, (b) 1900 MHz, (c) 3600 MHz, (d) 5000 MHz, and theta 90 deg. for (e) 5.9 GHz.

z-axis while keeping the distance between them fixed (120 mm). The results are shown in Fig. 15. The electric field components in magnitude and phase are exported and processed in MATLAB to calculate ECC and DG.

Figure 16 shows the calculations for ECC and DG at each rotation from the simulation data. By rotating the front PIFA, the distance between the feeding pin and shorting pin, and slots between the two elements are changed. Moreover, the intersection of the radiation pattern between the elements is modified which could help decrease the correlation between the antennas in the MIMO system depending on how the main beam is directed.

(a)

(b)

(c)

(d)
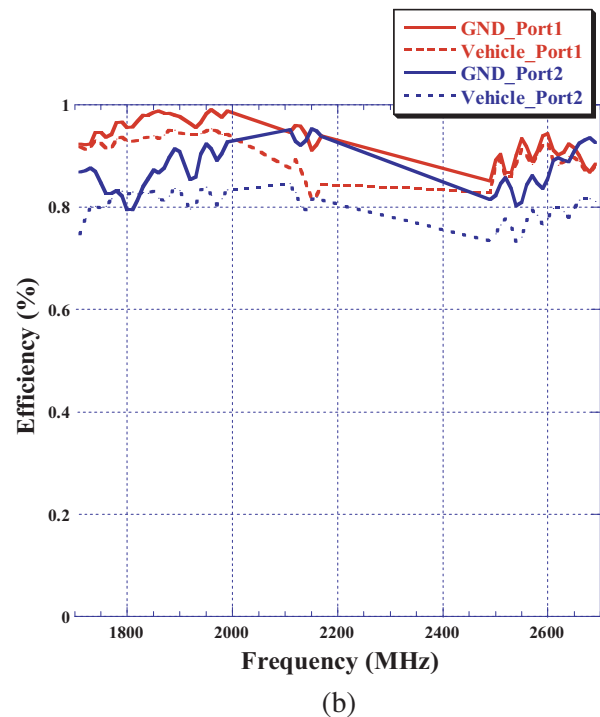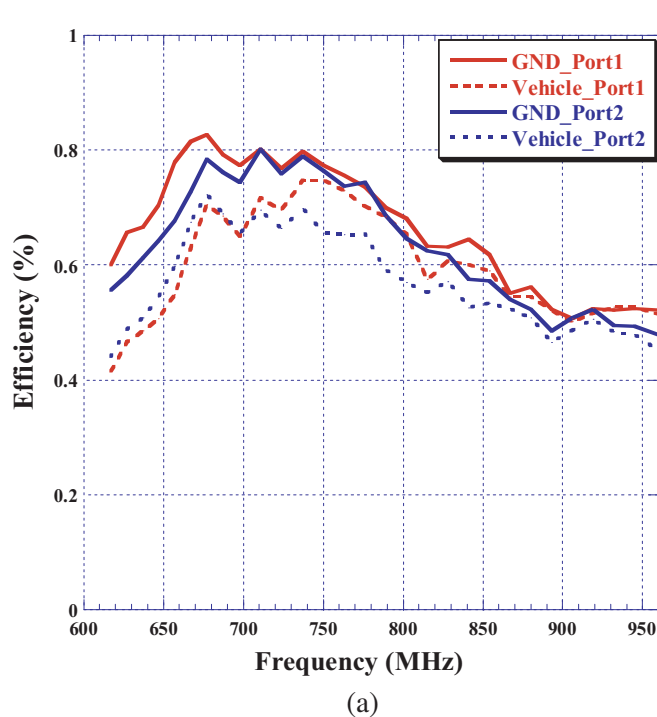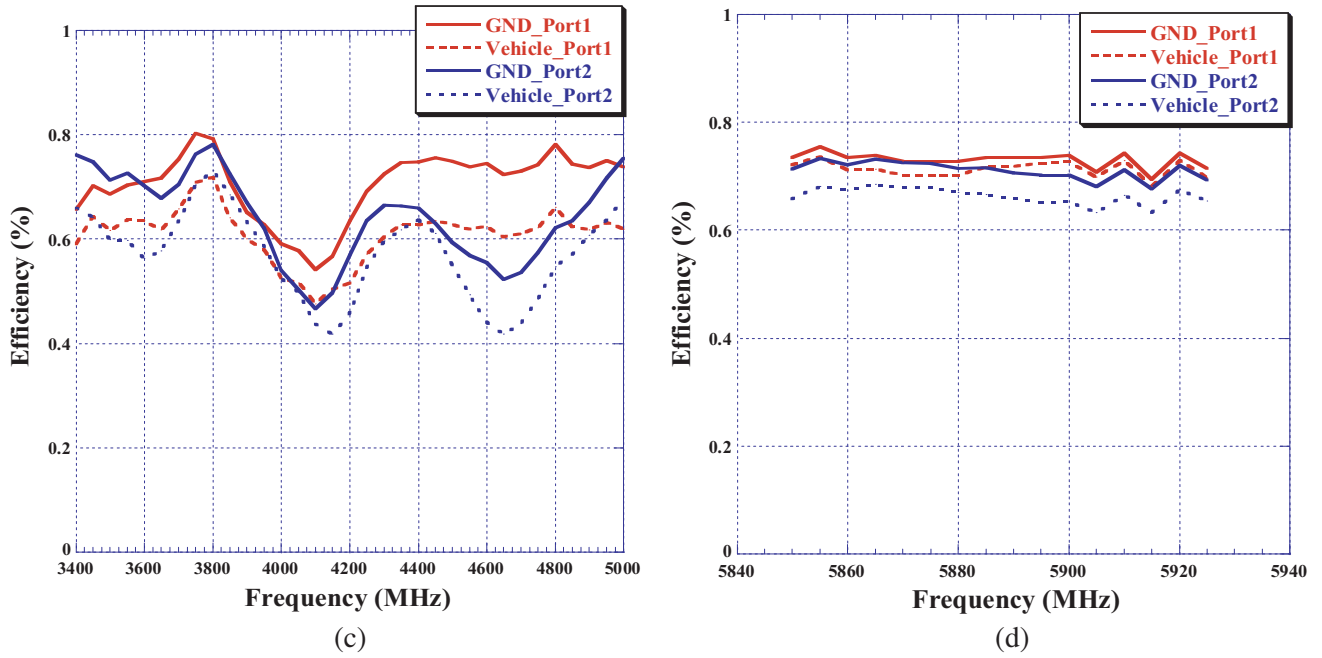
Figure 13. Antenna radiation efficiency for the two PIFAs: (a) 617 MHz–960 MHz, (b) 1710 MHz–2690 MHz, (c) 3400 MHz–5000 MHz, (d) 5850 MHz–5925 MHz.
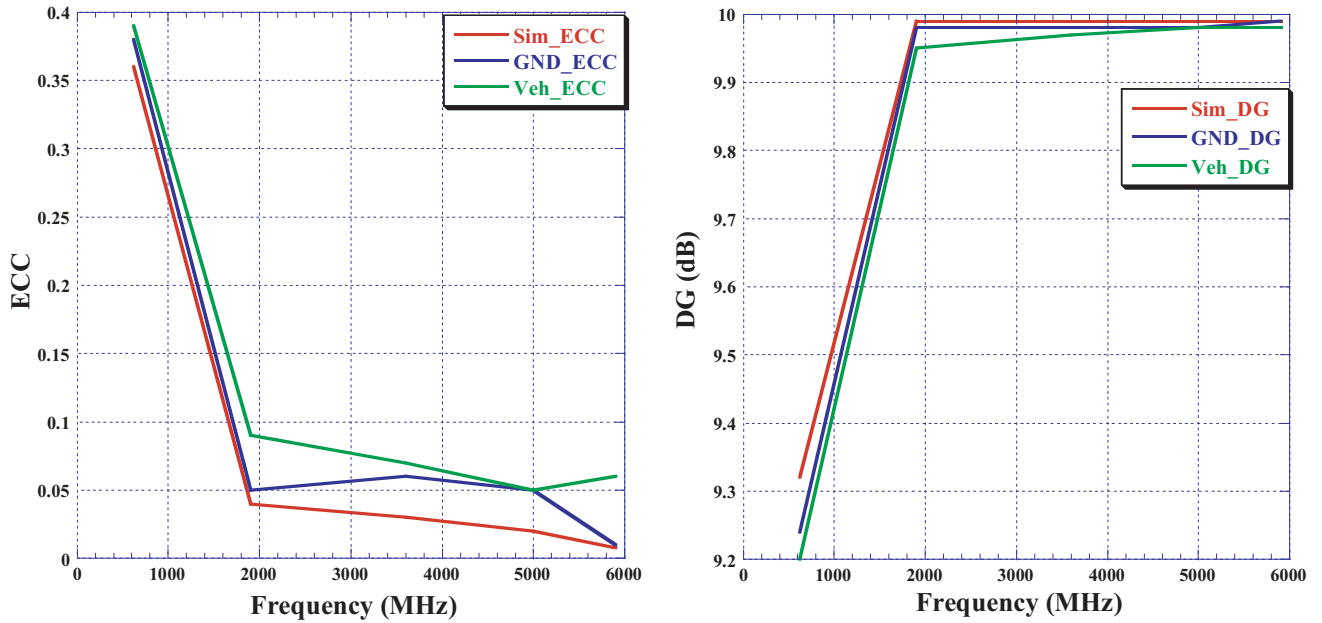
Figure 14. ECC and DG values for rotational MIMO System.

6. TWO-ELEMENT MONOPOLE-PIFA MIMO SYSTEM WITH ORTHOGONAL DIVERSITY

In this section, two antenna elements (monopole and PIFA) are placed on the same PCB with a distance of 120 mm (0.25 lambda of 617 MHz) between them. The proposed wide-band monopole covers the same 5G and V2X bands from (617 MHz–6 GHz) with reasonable physical dimensions to be used in a shark
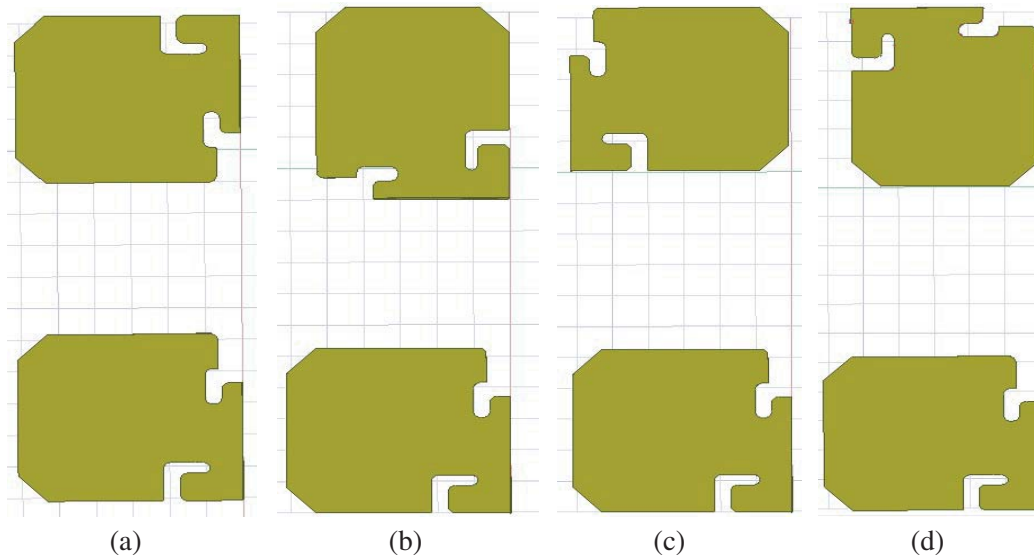
Figure 15. Top view of the MIMO antenna system with different rotational positions: (a) original position, (b) 90 degree shift clockwise, (c) 180 degree shift clockwise, and (d) 270 degree shift clockwise.
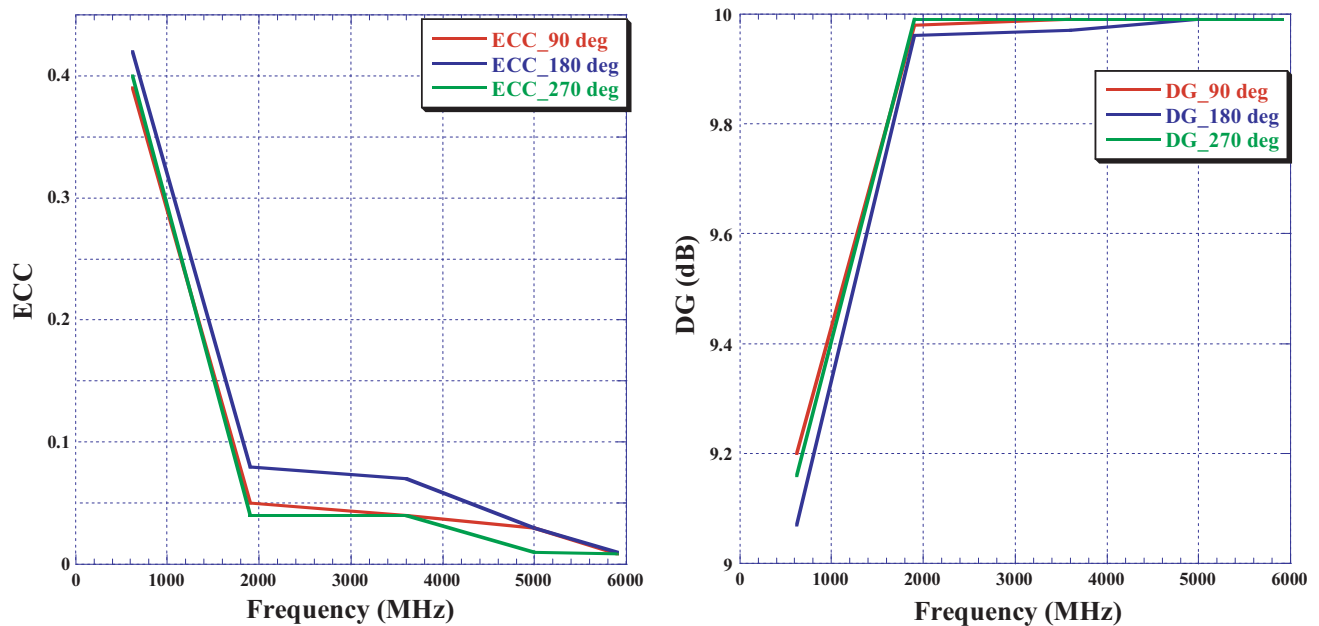
Figure 16. ECC and DG Values for different rotations.

fin housing. Fig. 17 shows the front and side views of the wide-band monopole design in addition to its distinct features and parameters with optimized values in Table 3. The monopole design consists of two unique branches: arm 1 and arm 2. The 5G low frequency band (617 MHz–960 MHz) is covered by arm 1 that operates as a folded monopole structure with a total radiating length of 96 mm which is $(\lambda/4)$ of the center frequency (780 MHz). The middle and high frequency bands for 5G and V2X (1.71 GHz–6 GHz) are attributed to arm 2 which is another wide monopole branch having a radiating length of 35.9 mm which is $(\lambda/4)$ of 2.08 GHz. The top loaded branch of arm 1 of width 14.9 mm increases the radiating length of the antenna to allow it to cover the lower frequencies. An L-shape slot structure exists between arm 1 and arm 2 to separate the low and middle frequency bands in order to reject the GNSS frequencies that resides between the two bands.

In this MIMO system, the monopole introduces a vertical surface current while the PIFA has some portion of the surface current on the horizontal plane specially at the low and middle frequency bands. The simulation and measurement setup on vehicle for this MIMO configuration is shown in Fig. 18.
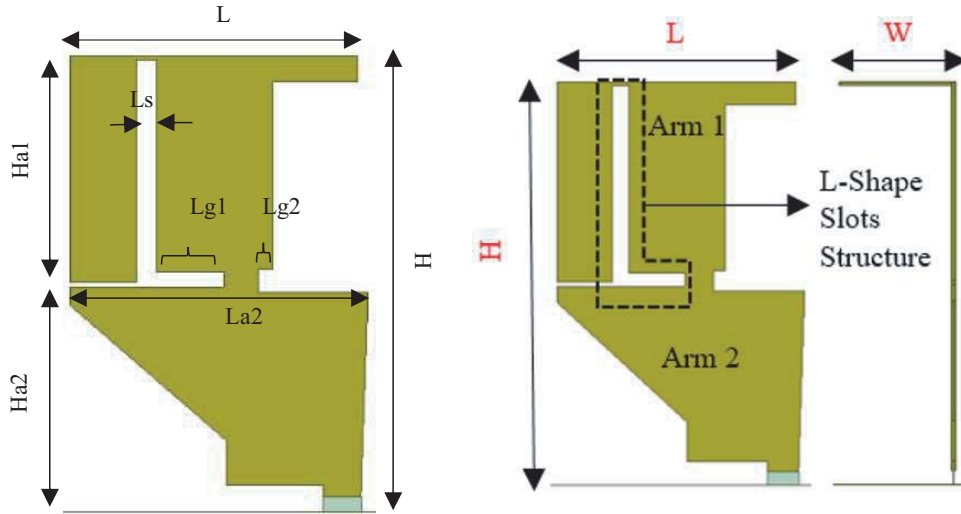
Figure 17. Compact monopole antenna with side and front dimensions.

Table 3. Values of different geometrical parameters of the wide-band monopole.

Parameter	Value (mm)	Parameter	Value (mm)
H	60	L_{g1}	9
L	38.5	L_{g2}	2
W	14.9	L_s	2.6
H_{a1}	30	L_{a2}	39.8
H_{a2}	29.3		
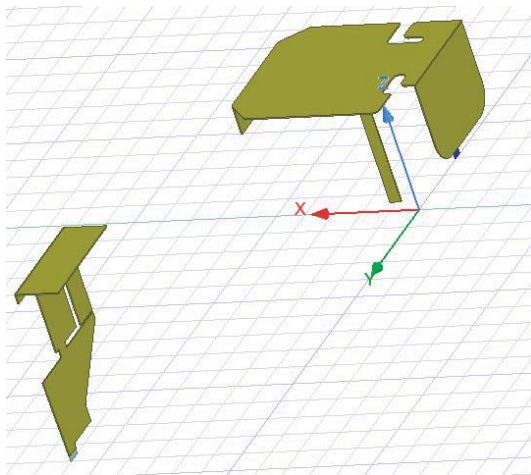
(a)   (b)

Figure 18. Measurement setup of the monopole-PIFA MIMO system on the vehicle. (a) Simulation setup. (b) Vehicle setup.

The elements are placed in the back center of the roof as in a shark fin module style.

The simulated VSWR for each element in this configuration is shown in Fig. 19. Ports 1 and 2 represent the monopole and PIFA, respectively. Both elements show a VSWR better than 3.3 : 1 across the 5G and V2X bands while also filtering out the GNSS bands. The passive isolation between the two elements is shown in Fig. 20. The worst-case isolation between the two elements has a value of 10 dB at the low frequency bands.

The combined radiation patterns for the two elements are shown in Fig. 21. The average gain observed from the combined vehicle radiation pattern is found to be -1.1 dBi, 2.3 dBi, 0.38 dBi, and
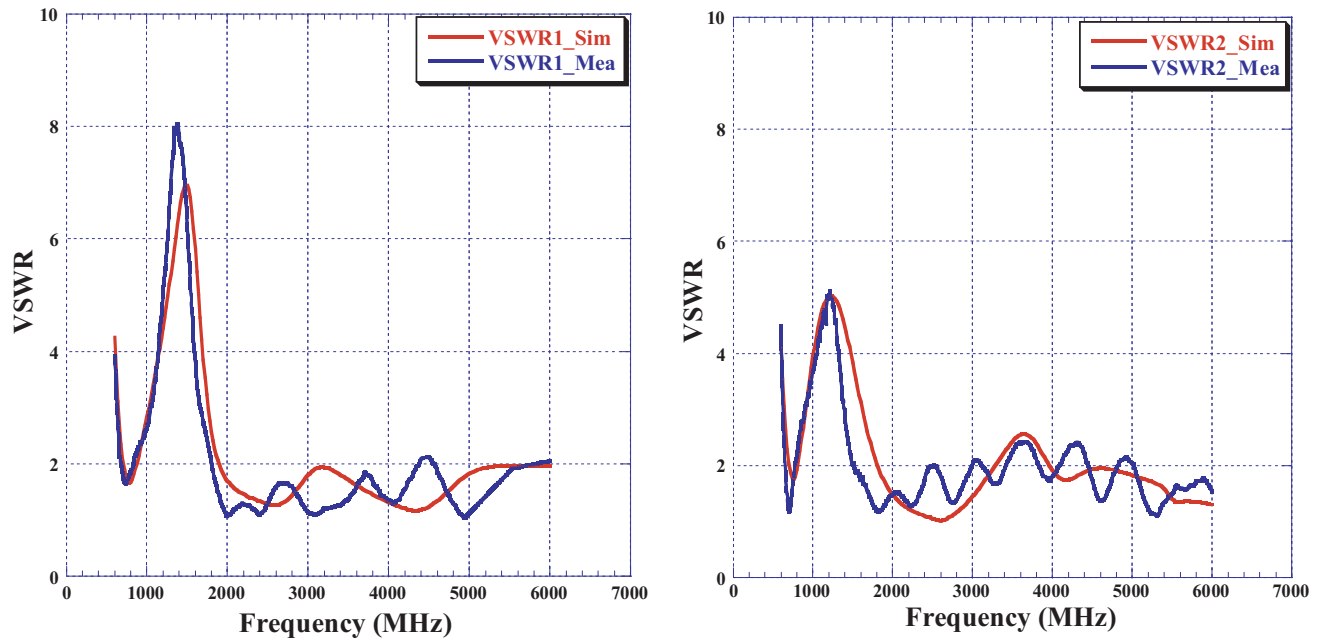
Figure 19. Simulated and measured VSWR for both elements.
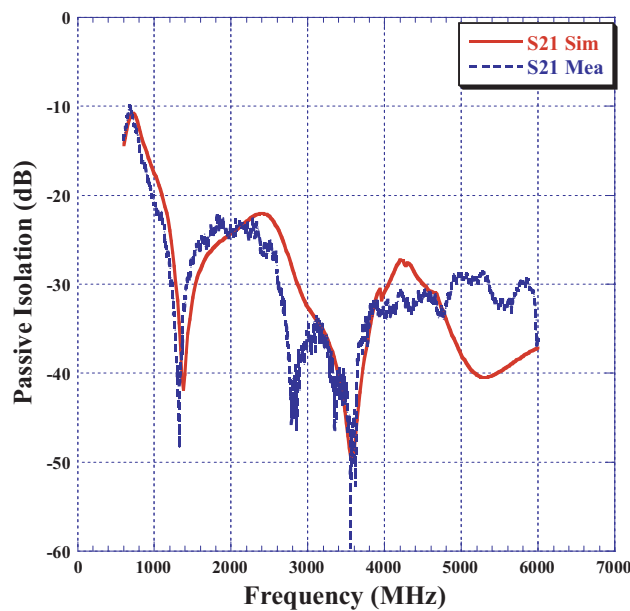
Figure 20. Simulated and measured passive isolation in dB.

0.97 dBi at frequencies 617 MHz, 1.9 GHz, 3.6 GHz, and 5 GHz, respectively. For V2X frequencies, at 5.9 GHz, the radiation pattern has a peak gain of 6 dBi at azimuth angle 225 degrees without having a minimum value lower than −11.2 dBi.

The measured radiation antenna efficiencies for the two elements are shown in Fig. 22. It can be noticed that the 5G GND measurement has an average efficiency higher than 72% for both elements across all frequency bands whereas the vehicle measurement has a reduced average efficiency of 64%. For V2X frequencies, the measured antenna efficiencies on GND and on vehicle are higher than 55% across the band.

The ECC and DG are also calculated in this MIMO configuration using Equations (1) and (2) with a MATLAB script. Fig. 23 shows these values. The worst values of ECC and DG exist in the low frequency band where the worst-case passive isolation exists between the two elements. Compared to the second configuration in Section 5, using the wide-band monopole yields better ECC and DG values. The improved ECC and DG performance can be attributed to having two partial orthogonal currents (horizontal current from the PIFA and vertical current from the monopole).

Next, a performance analysis is done via simulation by increasing the distance between the two

(a)   (b)

(c)   (d)

(e)
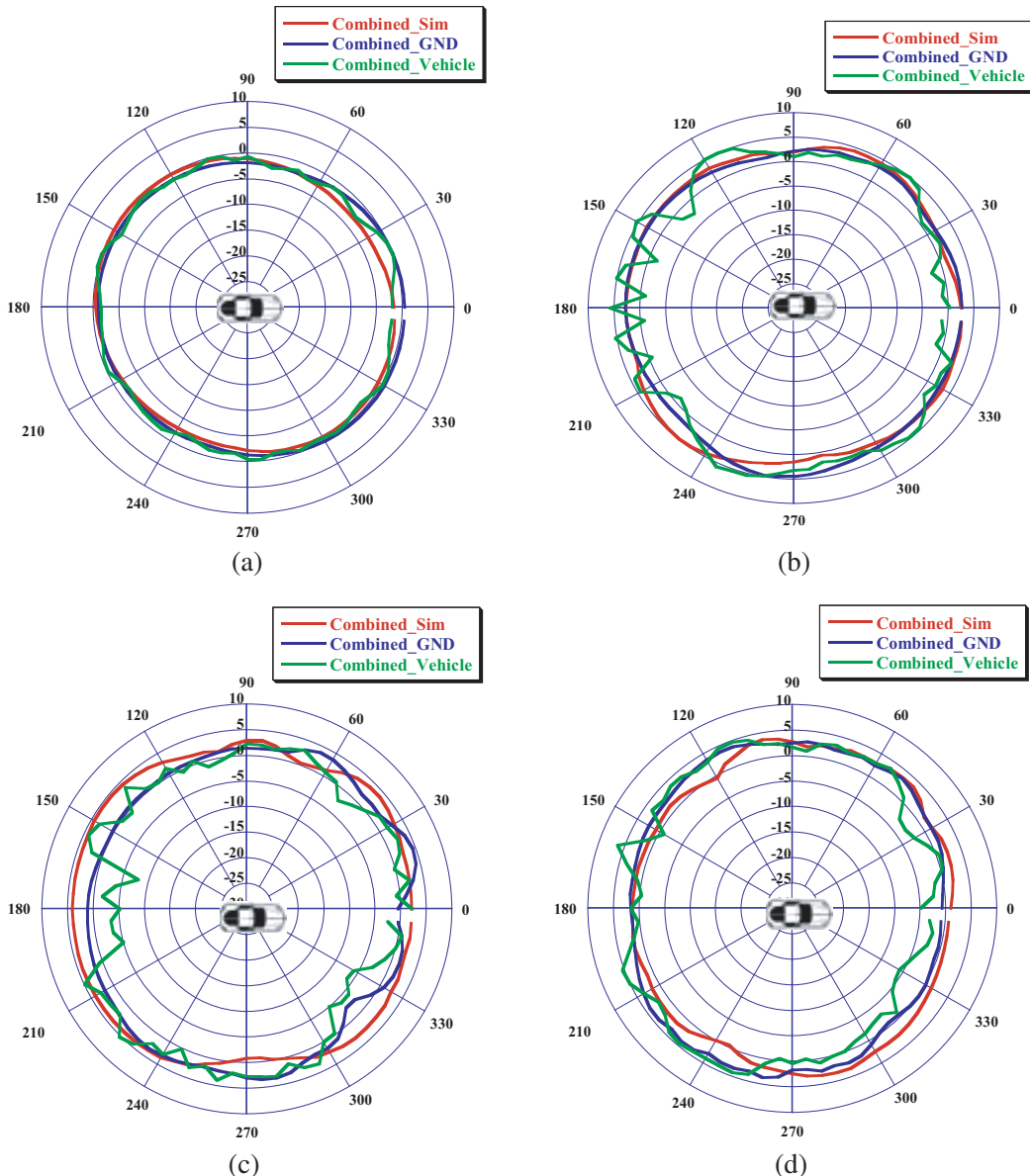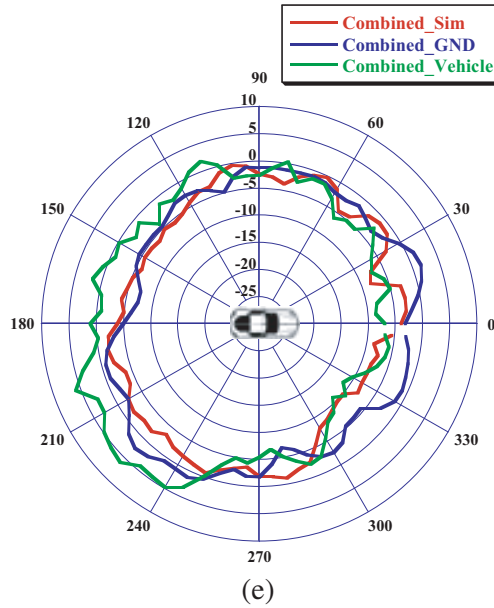
Figure 21. Combined Radiation pattern of simulation, GND measurement, and vehicle measurement in (dBi) at theta 80 deg. for frequencies: (a) 617 MHz, (b) 1900 MHz, (c) 3600 MHz, (d) 5000 MHz, and theta 90 deg. for (e) 5.9 GHz.

elements by 40 mm and rotating the PIFA by 90 degrees clockwise. First, the distance is changed to 160 mm between the elements while keeping the same orientation. The electric field components are exported and then processed in MATLAB to see the effect on ECC and DG. Fig. 24 shows the calculations done for ECC and DG at distance 160 mm, and it can be noticed that increasing the distance in this configuration improves the ECC and DG at the expense of package size.

(a)

(b)
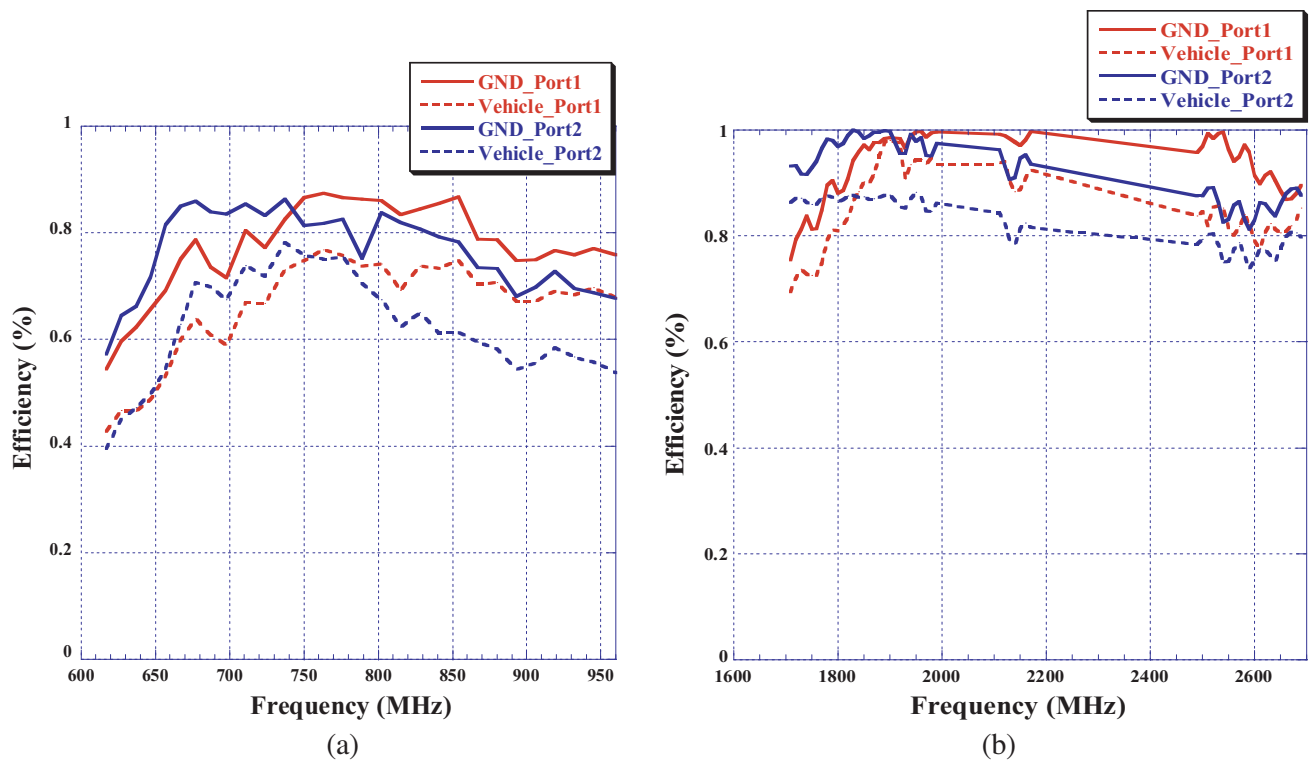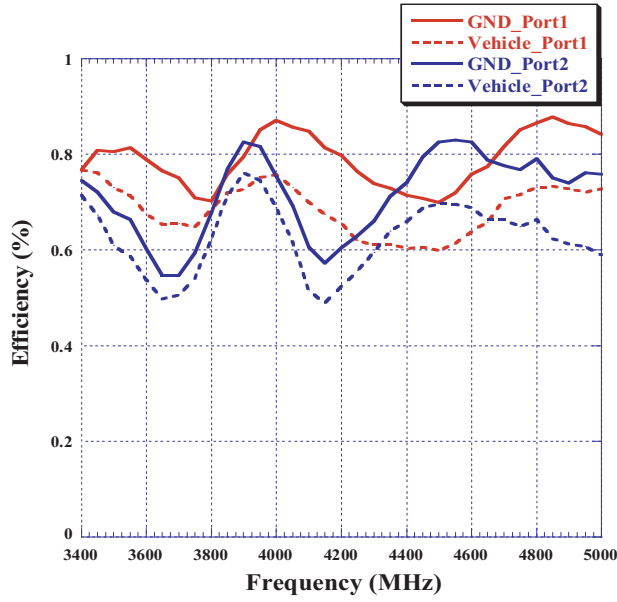
(c)
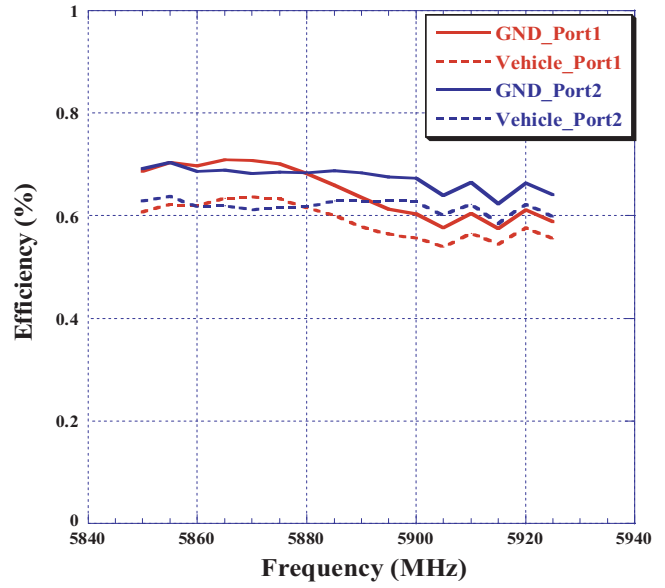
(d)

Figure 22. Antenna radiation efficiency for port 1 (monopole) and port 2 (PIFA): (a) 617 MHz–960 MHz, (b) 1710 MHz–2690 MHz, (c) 3400 MHz–5000 MHz, (d) 5850 MHz–5925 MHz.
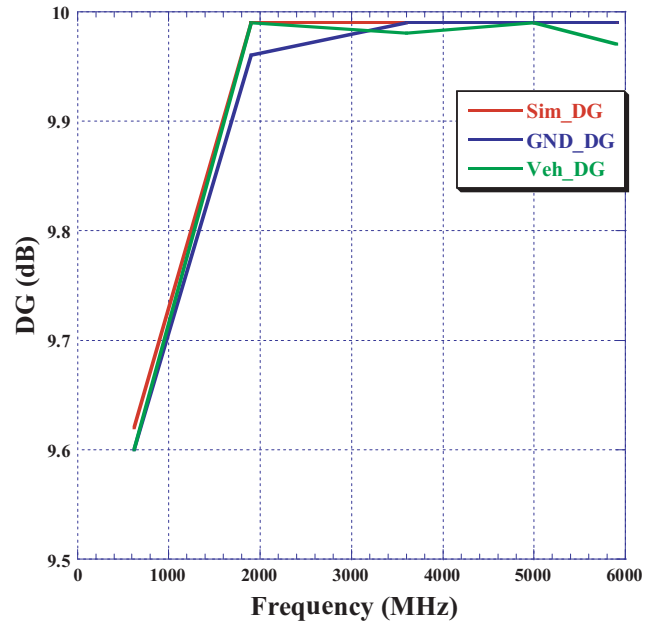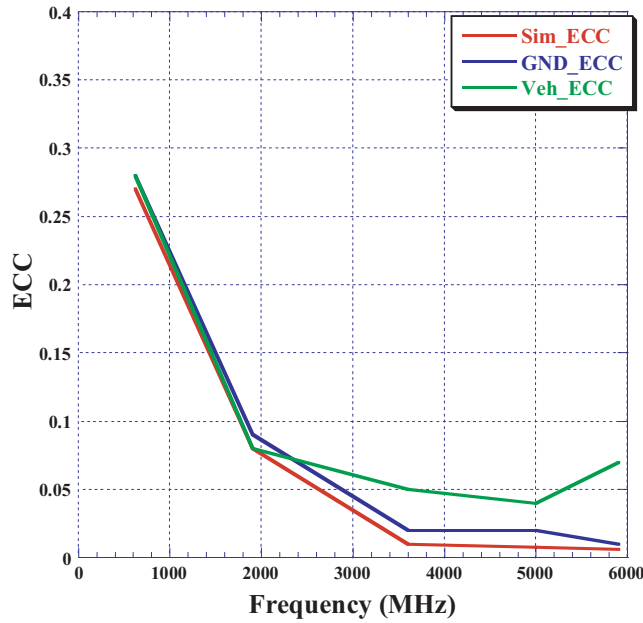
Figure 23. ECC and DG Values for PIFA-monopole MIMO system.

Figure 25 presents the values of ECC and DG when rotating the PIFA 90 degrees clockwise. There is a slight improvement in the low band frequency while the mid and high bands increase for the ECC. This could be reasoned from rotating the PIFA, and the shorting pin has moved further away from the monopole while the feeding pin gets closer to it, which might help in the low band isolation but not in the mid and high frequency bands.

Table 4 shows a literature review on the MIMO antenna systems used for automotive industry.

The table shows a comparison of the frequency band used in each system, physical dimensions of the elements, and how ECC is calculated in each work.
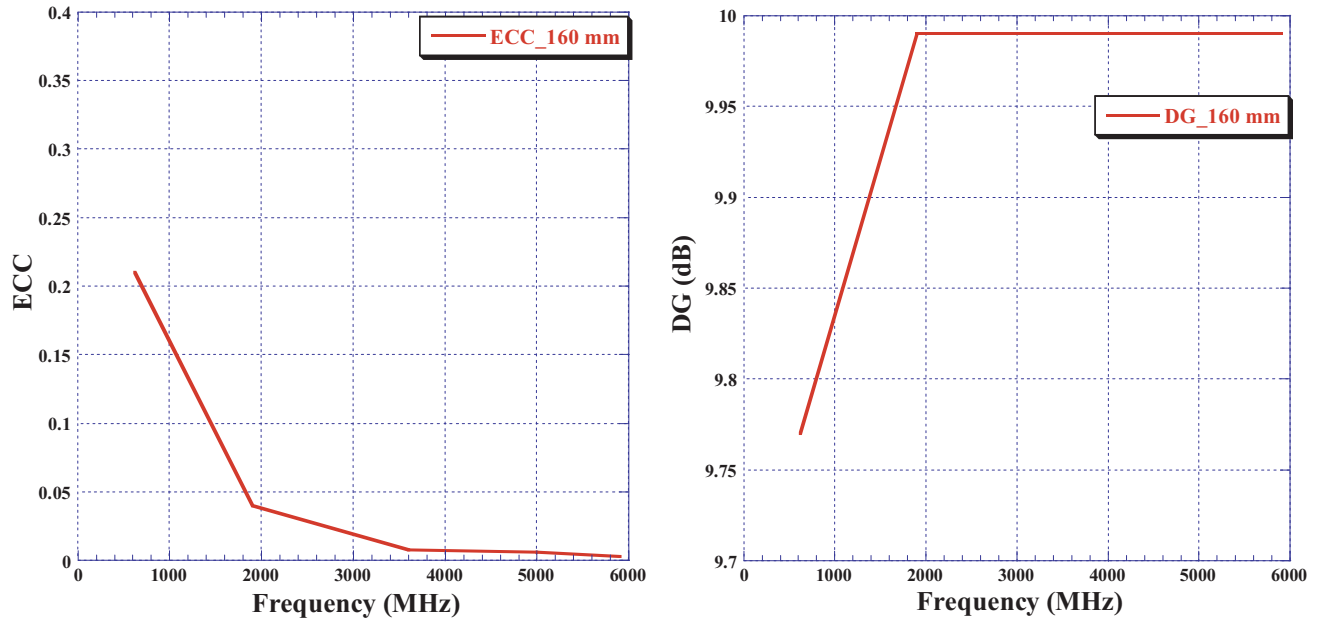
Figure 24. ECC and DG Values for at distance 160 mm.
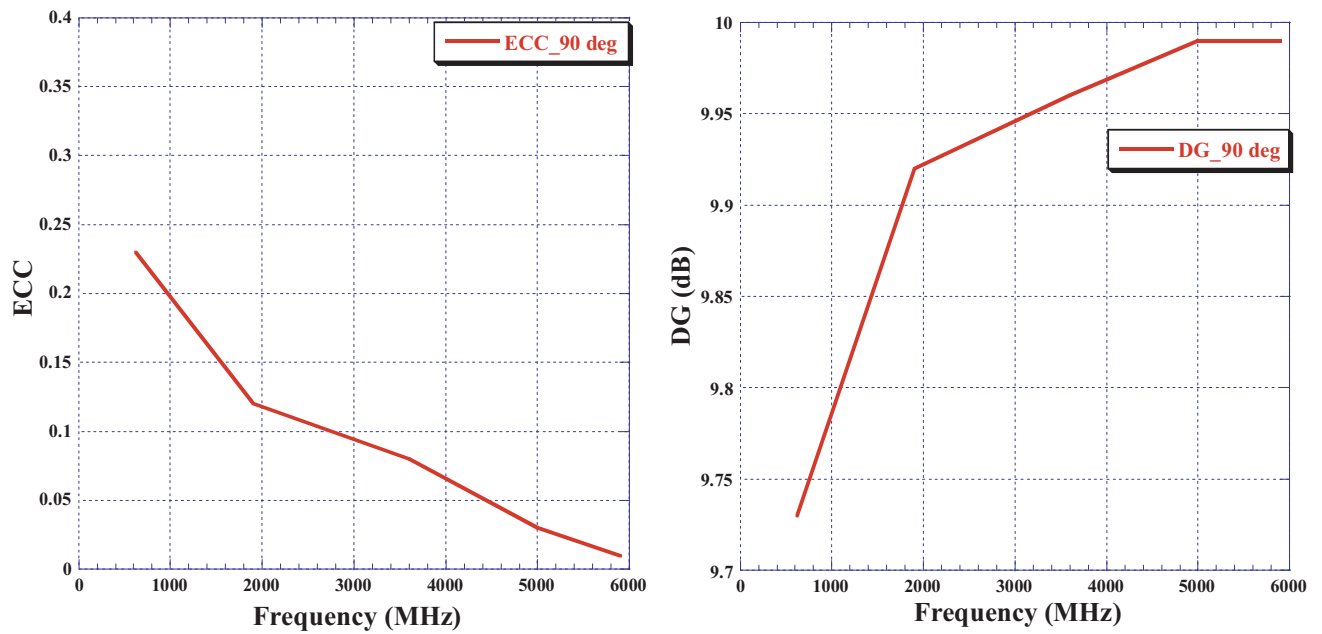
Figure 25. ECC and DG Values for at 90 degrees rotation.

Table 4. Literature review summary.

Ref.	Type	Bandwidth	Antenna Dimension $(L \times W \times H)$ (mm^3)	ECC method/ value
12	2×2 PIFA	775 MHz–925 HHz	$59.5 \times 12.4 \times 21$	S-parameter only/ lower than 0.5
13	2×2 printed Yagi	center frequency 3.5 GHz, bandwidth 600 MHz	$60 \times 1.6 \times 55$	Not reported/ lower than 0.5
14	2×2 PIFA	790 MHz–2.69 GHz	$50 \times 50 \times 28$	E field components/ lower than 0.3
15	2×2 Nefer Antenna	700 MHz–6 GHz	$70 \times 70 \times 29$	S-parameters only/ lower than 0.16
16	2×2 printed monopole	790 MHz–3 GHz	$30 \times 0.8 \times 80$	S-parameters only/ lower than 0.05
17	2×2 printed monopole PIFA	698 MHz–3 GHz	PIFA $65 \times 62 \times 20$/ Monopole height is 53.	Not reported
18	2×2 monopole	698 MHz–2.69 GHz	Back monopole height 55 mm/ Front monopole height 45 mm	S-parameters only/ lower than 0.5
19	2×2 PIFA	690 MHz–2700 MHz	PIFA length is 75.9 mm/ height 25.5 mm	S-parameters only/ lower than 0.5
20	2×2 monopole	700 MHz–900 MHz	Not reported	S-parameters only/ lower than 0.02
21	2×2 printed planar monopoles	698 MHz–2700 MHz	$52 \times 1.6 \times 65$	S-parameters only/ lower than 0.5
22	4×4 sleeve monopoles	790 MHz–5 GHz	Not reported	Not reported/ lower than 0.12
23	2×2 transparent semicircular slot-loaded monopoles	2.4 GHz–11 GHz	$24 \times 2.2 \times 29$	E-field components/ lower than 0.02
24	2×2 printed monopoles	698 MHz–2690 MHz	$25 \times 2 \times 55$	Not reported/ lower than 0.3

7. CONCLUSION

Multiple two-element based MIMO antenna systems are presented in this paper for 5G and V2X bands to be used in automotive applications. The ECC and DG values are calculated in each MIMO configuration using electric field components (magnitude and phase) from the radiation patterns of each antenna element. The first MIMO system represents two low profile PIFAs separated by a given distance (600 mm) on the vehicle's roof. The system achieves a passive isolation better than 26 dB, ports efficiencies higher than 68% on vehicle across all bands, ECC lower than 0.10, and DG higher than 9.94 dB. The second MIMO system consists of two PIFAs on the same PCB separated by a fixed distance and rotated in various positions. This MIMO system has a passive isolation better than 11 dB, ports efficiencies higher than 60% on vehicle, ECC lower than 0.39, and DG higher than 9.20 dB. Finally,

the third MIMO configuration investigates the performance when having one element as a monopole and one as PIFA. It achieves passive isolation better than 10 dB, ports efficiencies higher than 55% on vehicle, ECC lower than 0.28, and DG higher than 9.60 dB. In general, each MIMO configuration has a satisfactory performance and can be used in the vehicular applications depending on the desired requirement, housing style, and physical dimensions.

ACKNOWLEDGMENT

REFERENCES

1. Malik, J., D. Nagpal, and M. V. Kartikeyan, "MIMO antenna with omnidirectional pattern diversity," *Electronics Letters*, Vol. 52, No. 2, 102–104, Jan. 21, 2016.

2. Dama, Y. A. S., R. A. Abd-Alhameed, S. M. R. Jones, D. Zhou, N. J. McEwan, M. B. Child, and P. S. Excell, "An envelope correlation formula for (N, N) MIMO antenna arrays using input scattering parameters, and including power losses," *International Journal of Antennas Propagation*, Vol. 2011, Article ID 421691, 7 pages, 2011.

3. Elshirkasi, A. M., A. Abdullah Al-Hadi, M. F. Mansor, R. Khan, and P. J. Soh, "Envelope correlation coefficient of a two-port MIMO terminal antenna under uniform and Gaussian angular power spectrum with user's hand effect," *Progress In Electromagnetics Research C*, Vol. 92, 123–136, 2019.

4. Zhekov, S. S., A. Tatomirescu, E. Foroozanfard, and G. F. Pedersen, "Experimental investigation on the effect of user's hand proximity on a compact ultrawideband MIMO antenna array," *IET Microwaves, Antennas Propag.*, Vol. 10, No. 13, 1402–1410, 2016.

5. Sharawi, M., A. Hassan, and M. Khan, "Correlation coefficient calculations for MIMO antenna systems: A comparative study," *International Journal of Microwave and Wireless Technologies*, Vol. 9, No. 10, 1991–2004, 2017.

6. Arianos, S., G. Dassano, F. Vipiana, and M. Orefice, "Design of multi-frequency compact antennas for automotive communications," *IEEE Transactions on Antennas and Propagation*, Vol. 60, No. 12, 5604–5612, Dec. 2012.

7. Artner, G., W. Kotterman, G. Del Galdo, and M. A. Hein, "Automotive antenna roof for cooperative connected driving," *IEEE Access*, Vol. 7, 20083–20090, 2019.

8. Vaughan, R. G. and J. B. Andersen, "Antenna diversity in mobile communications," *IEEE Trans. Veh. Technol.*, Vol. 36, No. 4, 149–172, 1987.

9. Beegum, S. F. and S. K. Mishra, "Compact WLAN band-notched printed ultrawideband MIMO antenna with polarization diversity," *Progress In Electromagnetics Research C*, Vol. 61, 149–159, 2016.

10. Gao, Y., X. Chen, Z. Ying, and C. Parini, "Design and performance investigation of a dual-element PIFA array at 2.5 GHz for MIMO terminal," *IEEE Transactions on Antennas and Propagation*, Vol. 55, No. 12, 3433–3441, Dec. 2007.

11. Yacoub, A., M. Khalifa, and D. N. Aloi, "Wide bandwidth low profile PIFA antenna for vehicular sub-6 GHz 5G and V2X wireless systems," *Progress In Electromagnetics Research C*, Vol. 109, 257–273, 2021.

12. Kwon, O., R. Song, and B. Kim, "A fully integrated shark-fin antenna for MIMO-LTE, GPS, WLAN, and WAVE applications," *IEEE Antennas and Wireless Propagation Letters*, Vol. 17, No. 4, 600–603, Apr. 2018.

13. Kammakattu, S., P. Bora, M. Mudaliar, Y. Dhanade, and B. Madhav, "Linear array Yagi-Uda 5G antenna for vehicular application," *International Journal of Engineering & Technology*, Vol. 7, 513–517, 2017.

14. Franchina, V., et al., "A compact 3D antenna for automotive LTE MIMO applications," *2017 IEEE-APS Topical Conference on Antennas and Propagation in Wireless Communications (APWC)*, Verona, 326–329, 2017.

15. Hastürkoğlu, S., M. Almarashli, and S. Lindenmeier, "A compact wideband terrestial MIMO-antenna set for 4G, 5G, WLAN and V2X and evaluation of its LTE-performance in an urban region," *2019 13th European Conference on Antennas and Propagation (EuCAP)*, 1–5, Krakow, Poland, 2019.

16. Heiman, A., A. Badescu, and A. Saftoiu, "A new multiple input multiple output V2V automotive antenna for long term evolution band applications," *2018 International Symposium on Fundamentals of Electrical Engineering (ISFEE)*, 1–5, Bucharest, Romania, 2018.

17. Guan, N., H. Tayama, M. Ueyama, Y. Yoshijima, and H. Chiba, "A roof automobile module for LTE-MIMO antennas," *2015 IEEE-APS Topical Conference on Antennas and Propagation in Wireless Communications (APWC)*, 387–391, Turin, 2015.

18. Thiel, A., L. Ekiz, O. Klemp, and M. Schultz, "Automotive grade MIMO antenna setup and performance evaluation for LTE-communications," *2013 International Workshop on Antenna Technology (iWAT)*, 171–174, Karlsruhe, 2013.

19. Demien, C. and R. Sarkis, "Design of shark fin integrated antenna systems for automotive applications," *2019 PhotonIcs & Electromagnetics Research Symposium — Spring (PIERS-Spring)*, 620–627, Rome, Italy, 2019.

20. Song, H. J., et al., "Evaluation of vehicle-level MIMO antennas: Capacity, total embedded efficiency, and envelope correlation," *2014 IEEE-APS Topical Conference on Antennas and Propagation in Wireless Communications (APWC)*, 89–92, Palm Beach, 2014.

21. Preradovic, D. and D. N. Aloi, "Cross polarized 2×2 LTE MIMO system for automotive shark fin application," *The Applied Computational Electromagnetics Society (ACES)*, Vol. 35, No. 10, 1207–1216, Oct. 2020.

22. Jonah, O., "5G antenna for automotive applications," *2020 IEEE International Symposium on Antennas and Propagation and North American Radio Science Meeting*, 1493–1494, 2020.

23. Potti, D., et al., "A novel optically transparent UWB antenna for automotive MIMO communications," *IEEE Transactions on Antennas and Propagation*, 2020.

24. Liu, Y., Z. Ai, G. Liu, and Y. Jia, "An integrated shark-fin antenna for MIMO-LTE, FM, and GPS applications," *IEEE Antennas and Wireless Propagation Letters*, Vol. 18, No. 8, 1666–1670, Aug. 2019.